Design and Characterization of a Planar Mechanism for Passive Tilt-Compensation

by

Justin Yi-Shen Lai

Submitted to the Department of Mechanical Engineering
in partial fulfillment of the requirements for the degree of
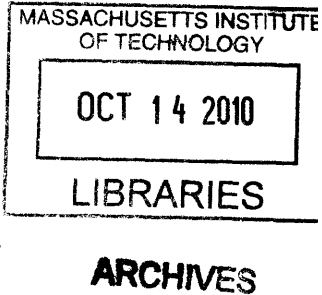
Bachelor of Science in Mechanical Engineering

at the

MASSACHUSETTS INSTITUTE OF TECHNOLOGY

May 2007
[June 2007]

Author ....
Department of Mechanical Engineering
May 11, 2007

Certified by...
Kamal Youcef-Toumi
Professor of Mechanical Engineering
Thesis Supervisor

Accepted by ....
John H. Lienhard V
Chairman of Undergraduate Thesis Committee

Design and Characterization of a Planar Mechanism for Passive Tilt-Compensation

by

Justin Yi-Shen Lai

Abstract

This work investigated the design and testing of a planar mechanism for passively compensating tilt between two flat surfaces brought into close proximity. The proposed design uses flexural components which eliminate friction and ensure smooth motion. To achieve this alignment in one of the two surfaces, two heights were fixed. The first height was fixed by a preload from a micrometer head. The second height was fixed by the clamping of a post. This was achieved by using a variation of an existing in-plane clamp design. After the post was clamped, the alignment from the conformal contact of the two surfaces was fixed. An error analysis is presented to estimate the uncertainty in the alignment. For experimentally characterizing the tilt error, capacitance probes were used to measure the alignment errors. It was found that the maximum uncertainty in the alignment was on the order of 50 μrad, making this design suitable for micro-scale planar alignment applications.

Thesis Supervisor: Kamal Youcef-Toumi
Title: Professor of Mechanical Engineering

Acknowledgments

THIS PAGE INTENTIONALLY LEFT BLANK

Contents

List of Figures

THIS PAGE INTENTIONALLY LEFT BLANK

Chapter 1

Introduction

1.1 Motivation

Small-scale gaps, on the order of nanometers, are important in many areas of science, specifically in the areas of biotechnology, DNA replication, and near-field physics studies. First, in the area of biotechnology, a means of filtration is necessary to separate particles for protein and nucleic acid research [10]. Current methods for the separation of biologically active molecules rely on chemical interactions, which could damage the sample in question [8]. If a small-scale gap can be created, then it can act as a mechanical filter, allowing molecules of certain sizes to pass through. A series of these filters could be cascaded to create the filtration scheme desired. Next, in the area of DNA replication, gaps formed on the level of nanometers create an ideal environment for a printing method called Supramolecular Nano-Stamping [22]. Finally, a small scale environment provided by instrumentation could prove useful for the study of radiation heat transfer and near field physics [11]. Developing such technology could unlock research fields in many disciplines.

1.2 Mechanical Engineering Approach

In this section, the mechanical engineering approach to the creation of small-scale gaps is discussed.

1.2.1 Primary Concerns

This approach to the problem is to use closed-loop control to actively control the gap of two plates. There are three primary concerns within this problem:

- Surface finish of two plates

- Programmability of gap

- Accounting for tilt error

First, the surfaces need to be optically flat, since a gap on the nanometer scale are desired. Next, the gap needs to be adjustable, according to the desired height. The range of motion and the resolution of adjustment are key concerns. Finally, systematic errors can produce differences in the angles between the two surfaces. Note that the gap of nanometers is created across the length scale of centimeters. Figure 1-1 illustrates the high aspect ratio in this problem.
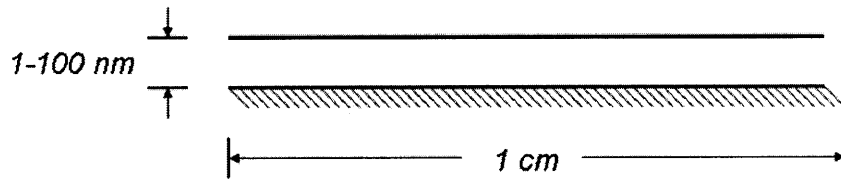
Figure 1-1: Aspect ratio of height to width

1.2.2 Active Compensation

Active compensation involves the use of three sensors and three actuators to actively control the height of the gap. Capacitance probes, with a resolution on the order of 10 nm, can sense the three distance readings and a controller can compensate until the two surfaces are parallel. There are several examples of previous work which deals with small-scale manipulation and alignment, using active feedback control to gain desired behavior of the degrees-of-freedom of pitch and roll [6, 21, 12].

However, in this study, we wanted to take the passive approach for the alignment of the two surfaces. Taking this path provided for a simpler system, with less sensors and actuators to manage. Once we reached the desired orientation, we wanted the angle to be locked. Then, we were only concerned with the active control of the gap height.

1.3 Passive Tilt-Compensation

This section discusses the basics of passive tilt-compensation and the experimental goal in this study. Our method of passive tilt-compensation involved the conformal contact of two surfaces. Shown in Figure 1-2, the first surface was at some given angle θ, with respect to the top surface. As the top surface moved towards the bottom, it eventually made contact with the bottom side. This initial contact point became a pivot point. Then the top surface continued to pivot until the two surfaces mated. Using capacitance probes parallelism was assessed.
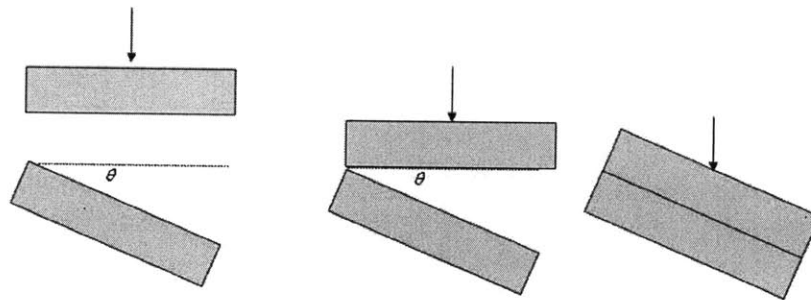
Figure 1-2: Conformal contact in passive-tilt compensation

We desire to design and fabricate an instance of this concept that will achieve this passive tilt-compensation. After this mating is formed, the angle must be locked somehow. Once the angle is fixed, the preload force on one of the surfaces is then released, bringing back one of the two surfaces. The gap is then formed, with the two surfaces ideally parallel. The preload force maintains the conformal contact. With the release of the preload force, however, there could be a deviation from the parallel

orientation formed while the surfaces are mated. It is desired to minimize any change that will occur.

1.4 Mechanical Locking

This section discusses a mechanical way of maintaining the angle formed after conformal contact. Specifically in this thesis, we investigated the mechanical locking of a rigid post to maintain the angle after the conformal contact had occurred. In order to isolate the study, the scope of this investigation was limited to the alignment of one degree of freedom in a planar mechanism. In Figure 1-3 the degree of freedom is θ_z while the x and y coordinates are in plane.
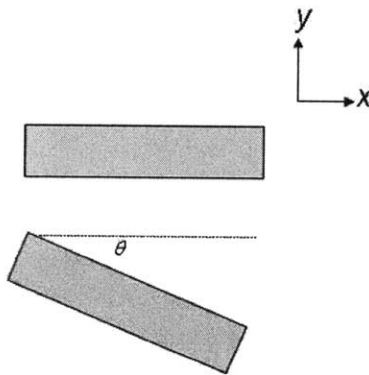
Figure 1-3: Coordinate system for tilting

The connection from the post to the top surface must be rotationally compliant. Figure 1-4 through 1-7 shows the kinematics the conformal contact, with the rigid post which has the rotationally compliant joint. These schematics diagrams are meant to portray things in a general sense. We used flexural joints instead of pin or friction joints, as illustrated in the figures, in order to ensure smooth motion.
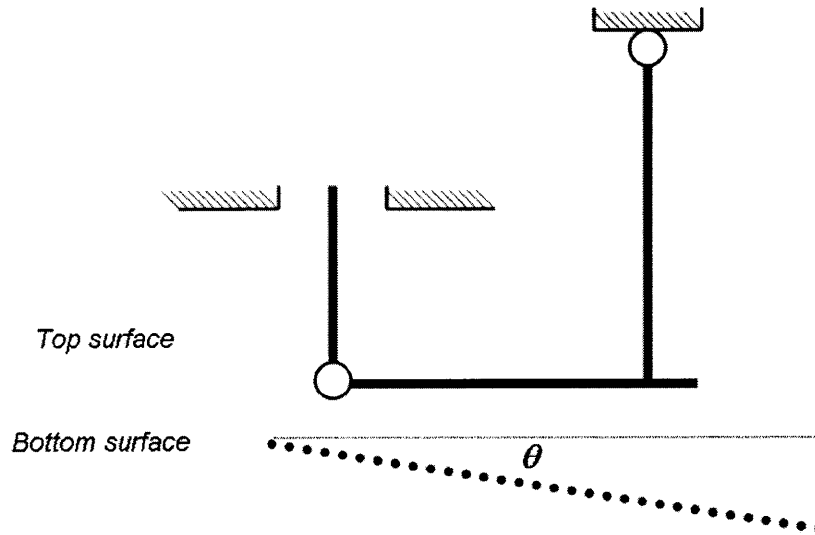
Figure 1-4: Initial state, when two surfaces are at different angles; circles represent flexural pivots

1.5   Goal

The goal of this work was to characterize the performance of the mechanical clamping of a rigid post to maintain the angle formed by passive tilt-compensation. From the clamping of the post, there was a deviation from the angle formed during conformal contact. Possible sources of angular displacement were from the temperature variation, elastic springback, and the Poisson's ratio as the post was being clamped. Experiments were conducted to characterize the uncertainty of the alignment after the proposed method was implemented for tilt-conmpensation. The results revealed the appropriate applications for this implementation of programmable small-scale gaps. Figure 1-8 shows the full assembly used in the experiments, without the capacitance probes. Figure 1-9 shows the capacitance probes close up.

Actuation-preload force
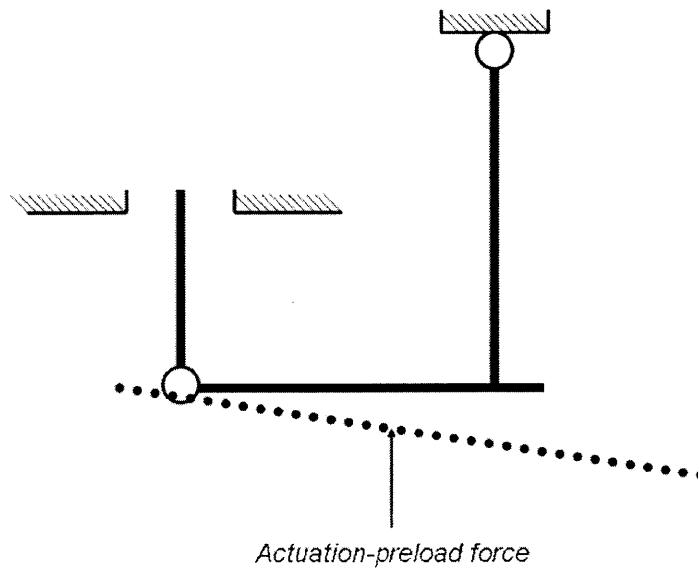
Figure 1-5: Initial contact made between two surfaces, contact point becomes pivot point

Mechanical locking

Conformal contact made
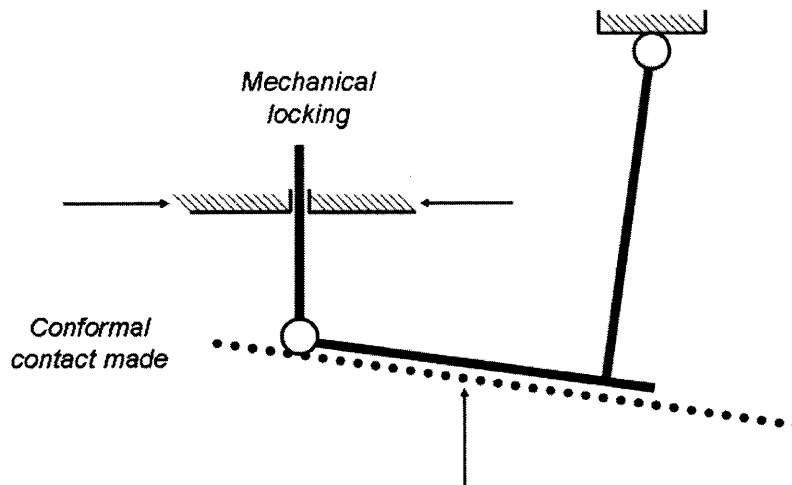
Figure 1-6: Conformal contact created, angle locked
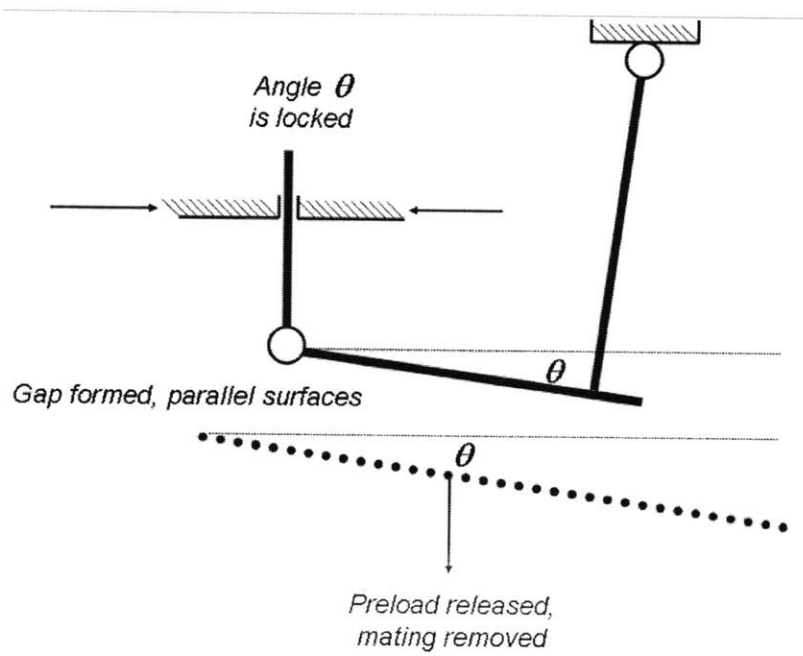
Figure 1-7: Preload released and gap formed with ideally parallel surfaces
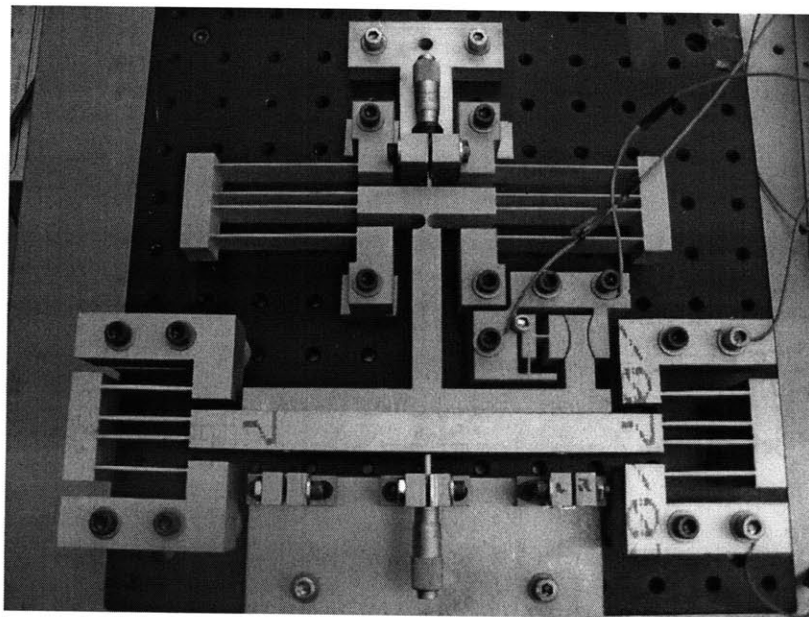
Figure 1-8: Picture of overall assembly used in experiments, without capacitance probes
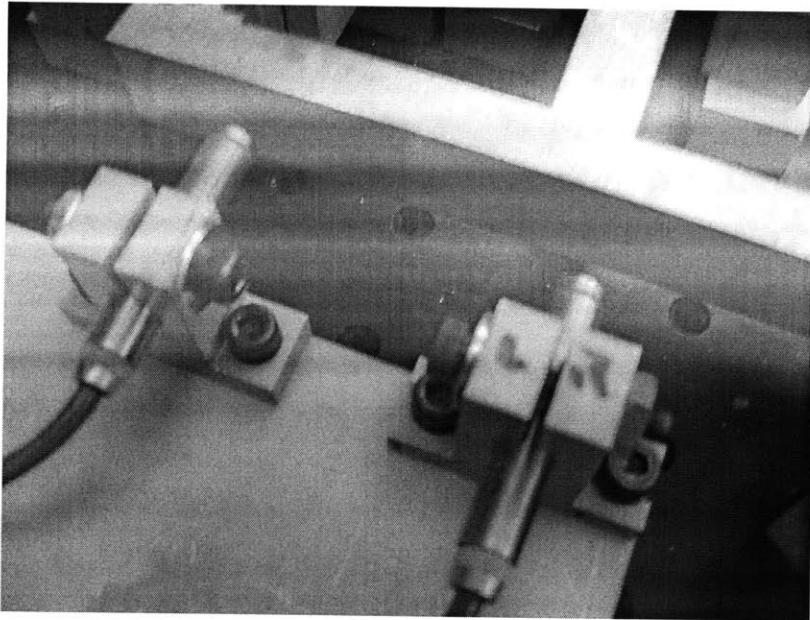
Figure 1-9: Close-up of capacitance probes during experiments

Chapter 2

Design

2.1 Introduction

This chapter documents considering prior art, modeling the system based on functional requirements, and using computer simulations to determine the dimensions for the system.

2.2 Prior Art

This section will discuss the ideas and concepts upon which this study is built. This thesis was carried out as part of ongoing research at the MIT Mechatronics Research Laboratory, on programmable small-scale gaps [8, 7, 16, 17, 15].

2.2.1 Literature Review

Our literature review began with Mauricio Guiterrez's Master's thesis, where he designed instrumentation to create a programmable gap in order to filter biologically active molecules [7]. Also, studies have been done to model and analyze the control of this system [16, 17]. In this work, a piezoelectric actuator pushed down on a universal circular flexure, which conformed to a bottom plate. Figure 2-1 is a picture from this earlier iteration of the instrumentation.
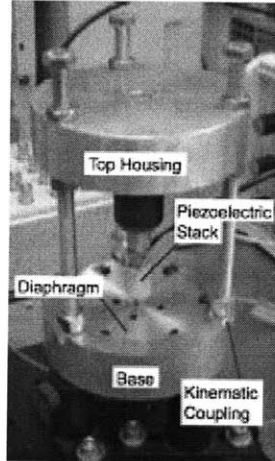
Figure 2-1: Picture of experimental setup from previous iteration of adjustable-gap instrumentation, courtesy of Gutierrez [7]

The next step for this line of work was to investigate the locking of the angle after conformal contact. It was proposed to use epoxy, made of the same material as the universal circular flexure. Once the two plates would be, epoxy would be injected into a reservoir around the flexure. After it hardened, the angle would be fixed. The preload of the actuator would be released and the gap would be formed.

2.2.2   Continuing for Previous Work

In bench-level experiments of the curing of the epoxy, however, we discovered that it was not feasible for the project. The curing time was too long and it was difficult to get uniform distribution of ultra-violet light onto the flexure and reservoir.

A new way to lock the angle was needed. We came up with an idea to use a rigid post with a notch flexure connected to the top surface. A planar clamp provided the means for holding the position of the post, mechanically locking the alignment. The advantage with this approach is that the flexure relies on elastic deformation for compliance, allowing it to be used repeatedly. With epoxy hardening, the flexure couldn't be reused after the epoxy solidifies. As long as the flexure is deformed within its elastic limits, the flexure can be used multiple times.

2.3   Functional Requirements for Experimental Setup

This section discusses the functional requirements for the experimental setup. For this experiment, we focused our study on the clamping of the rigid post for locking the angle. Therefore, we desired to make the system and instrumentation as simple as possible. Further, we also desired to minimize the amount of machining yet make it usable for other studies in the future. The functional requirements were:

- Planar mechanism

- Monolithic frame

- Modular components for future use and experiments

2.4   Flexural Mechanisms

This section discusses the various flexural mechanisms employed in this design. Previous work, that involved both active and passive compensation used flexural elements [6, 21, 12, 18]. Work done on designing micro-manipulaton systems used notch flexures to reduce macroscopic inputs [20]. Also, planar mechanisms were used to mate surfaces in the area of flash-imprint lithography [5]. In short, flexures are the appropriate elements for our system because it allows for smooth, continuous motion, within the elastic limit of the material [9, 19].

Specifically, the following three flexural elements were used in our system, after examining how it was used in previous work [2, 4, 1].

2.4.1   Double Parallelogram

The double parallelogram allows motion in the y-direction of the system to have virtually zero parasitic errors in angle [4]. The intermediate stage absorbs any sort of motion in other directions and guarantees motion only in the actuated direction. Equation (2.1) is the transverse stiffness for the double parallelogram shown in Figure 2-2 based on work done by Awtar [4].

$$k_y = \frac{12EI}{L^3} \tag{2.1}$$

where E is the Young's Modulus, I is the bending moment of inertia of the blades of the parallelogram and L is the length of the blade.
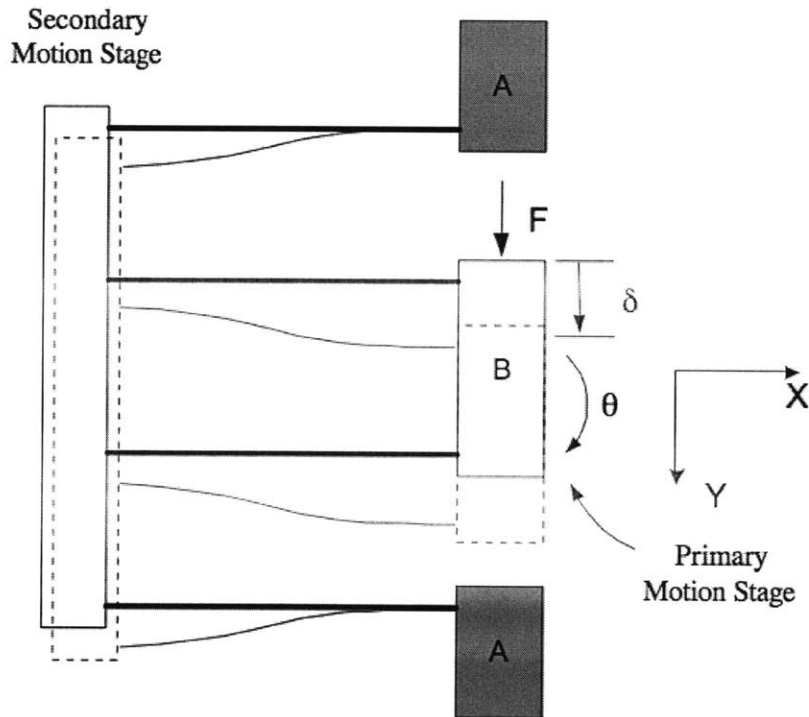
Figure 2-2: Diagram of double parallelogram structure, courtesy of Awtar [4]

2.4.2 In-plane Clamp

A planar clamp was designed by Awtar to safely house capacitance probes for in-plane measurements [3]. This flexural element was adapted to mechanically clamp the post, once conformal contact occured. Two flexures allow for moments at the hinges, creating distributed loads on the clamped element, coming from the force from the tapered pipe plug. The pipe plug creates the clamping force, as it is turned downwards. Figure 2-3 illustrates the in-plane clamp holding a cylindrical object.
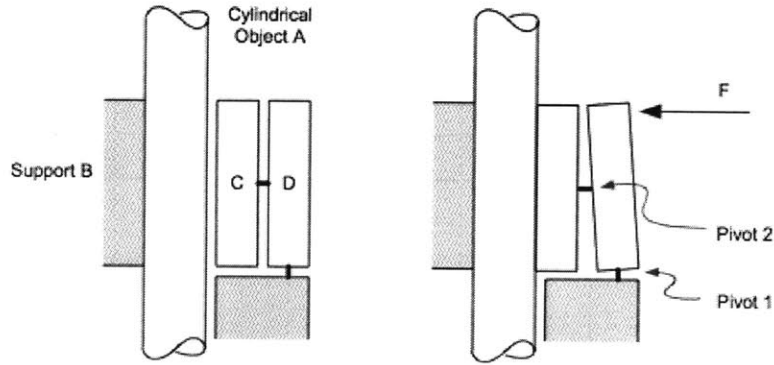
Figure 2-3: Schematic of in-plane clamp, courtesy of Awtar [3]

2.4.3 Notch Flexure

A simple notch flexure was used in order to provide rotational compliance with high axial stiffness [19]. The rotational stiffness is given by Equation (2.2). Figure 2-4 shows the notch flexure.
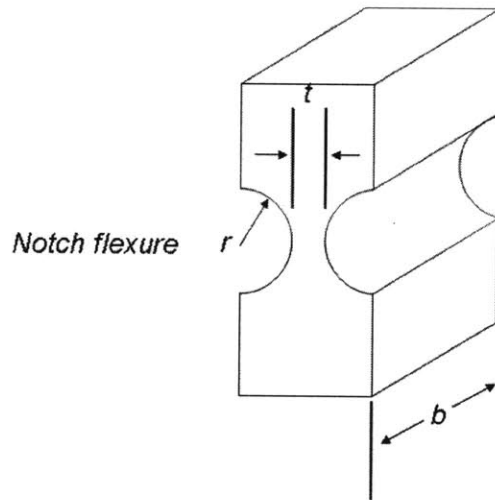
Figure 2-4: Notch flexure

$$k_{notch} = \frac{2Ebt^{5/2}}{9\pi r^{1/2}}$$

(2.2)

2.5 System Model

This section describes the various properties and behaviors needed from the system.

2.5.1 Characteristics

The different aspects of the system were the key variables listed here:

- θ_{error} - Initial misalignment

- $\theta_{compensation}$ - Rotational range of tilt-compnesation mechanism. Ideally displaces to meet θ_{error}

- Actuation for conforming

- Actuation for preload and release

Figure 2-5 shows the coordinate system again.
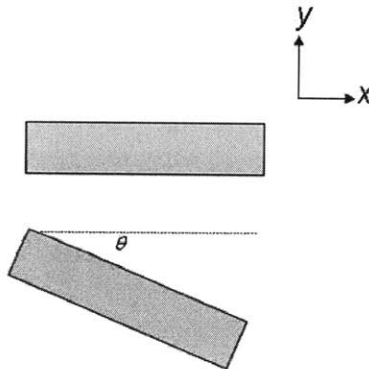
Figure 2-5: Coordinate system for tilting

One of the components needed the means to comply to the other surface, allowing both surfaces to mate with each other. There needed to be a means to push one of the components in the y-direction to force this compliance. Also, there needed to be a sufficient preload or stiffness in the y-direction to only allow rotation.

2.5.2 Top Module

The system was divided into two halves, a top and bottom module In the top module, we decided to use a micrometer head to make a coarse adjustment. It acted on the double parallelogram, which ensured motion only in the y-direction. A notch flexure was placed between the main stage of the top double parallelogram and the rigid link which connected to the top surface. This to allowed for rotational compliance, as the top surface mated to the bottom surface.

The micrometer head mentioned created a preload at the top as shown in Figure 2-6. This fixed the first height. Once the conformal contact occurred, the in-plane clamp fixed the post, thus holding the second height. These two fixed heights determined the angle of the top surface. Figure 2-7 adds the in-plane clamp to the assembly.
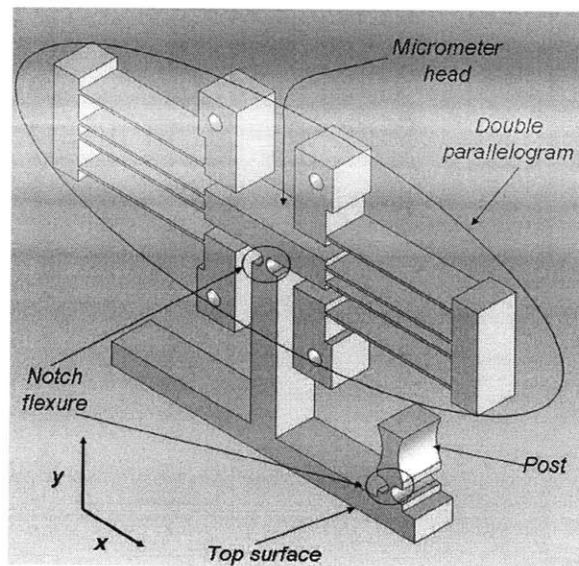
Figure 2-6: Top module, with various flexural elements

2.5.3 Bottom Module

The bottom module was the mechanism to force the top surface to conform to the bottom surface. Also, it was planned to have a piezoelectric actuator used as a fine adjustment, acting at the center of the bottom module. The double parallelogram here was designed to be axially and rotationally stiff, so that it would maintain its

29
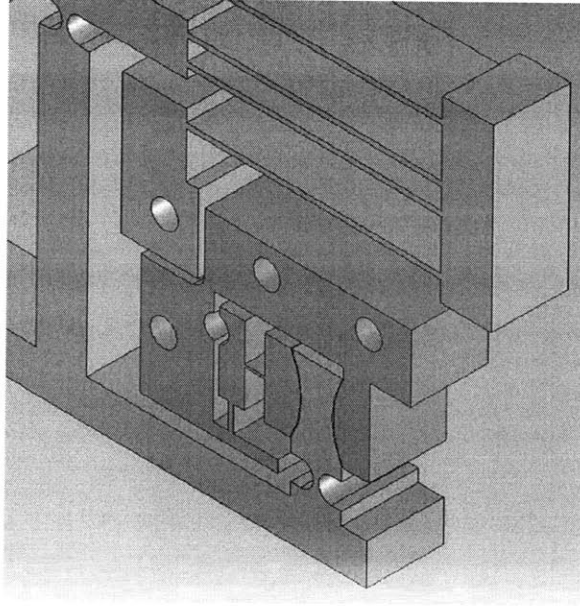
Figure 2-7: In-plane clamp with post

angle as it made contact with the top module. The actuator making the second adjustment became a preload to force the two surfaces to contact and mate. Two capacitance probes measured the displacement of the top surface. Figure 2-8 shows the bottom module.

2.6 Kinematics of Contact

This section describes the time history of the system in motion.

2.6.1 Initial Condition

Initially, the bottom surface is at some given angle θ. The post on the left-hand side is not a free pivot, but rather a rotationally compliant joint, when a force is applied. Figure 2-9 shows this state.
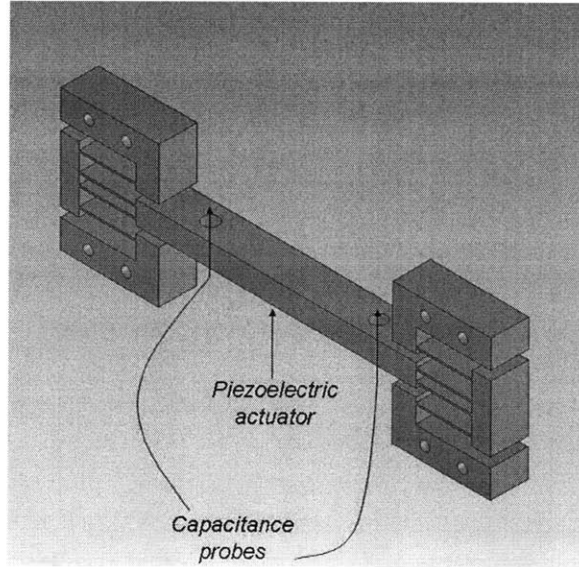
Figure 2-8: Bottom module

2.6.2 Initial Contact Made

A preload force is applied onto the bottom module, bringing it towards the top module, maintaining the angle θ. The first point of contact becomes a pivot point. Figure 2-10 shows this state.

2.6.3 Conformal Contact, Angle Locked

Now the two surface are mated. The rotational joint between the post and the top surface allows the top module to conform to the angle of the bottom module. The post is now locked mechanically. Figure 2-11 shows this state.

2.6.4 Preload Released, Gap Formed

Finally, the preload is released from the bottom module. Now both surfaces are ideally at the same angle. Figure 2-12 shows this state.

Top surface

Bottom surface

θ
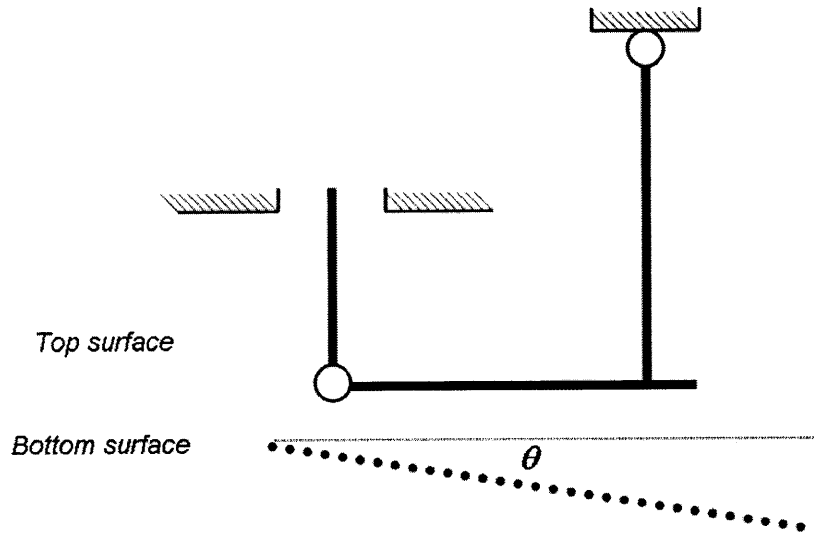
Figure 2-9: Initial state, when two surfaces are at different angles

Actuation-preload force
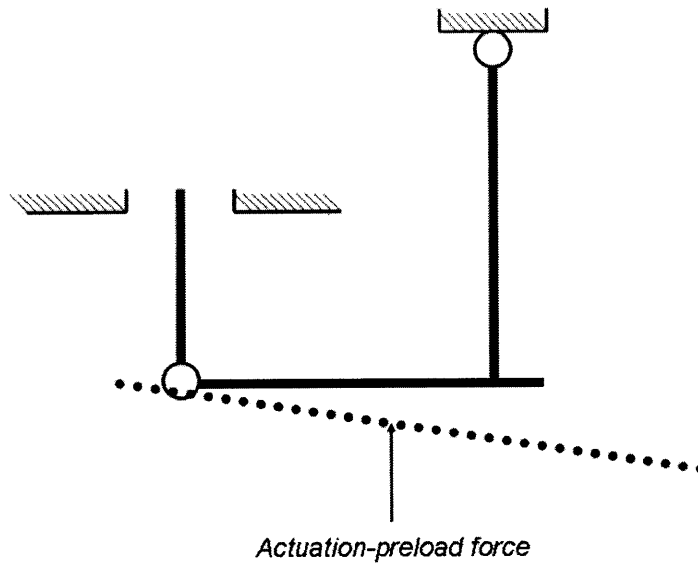
Figure 2-10: Initial contact made between two surfaces, contact point becomes pivot point
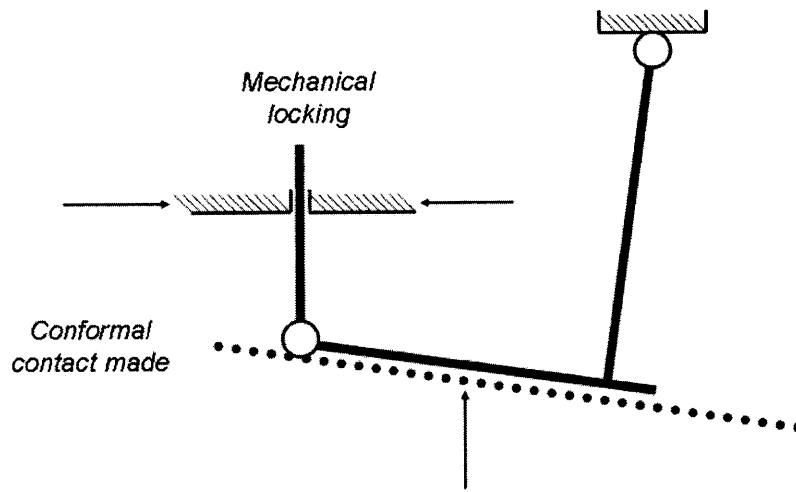
Figure 2-11: Conformal contact created, angle locked
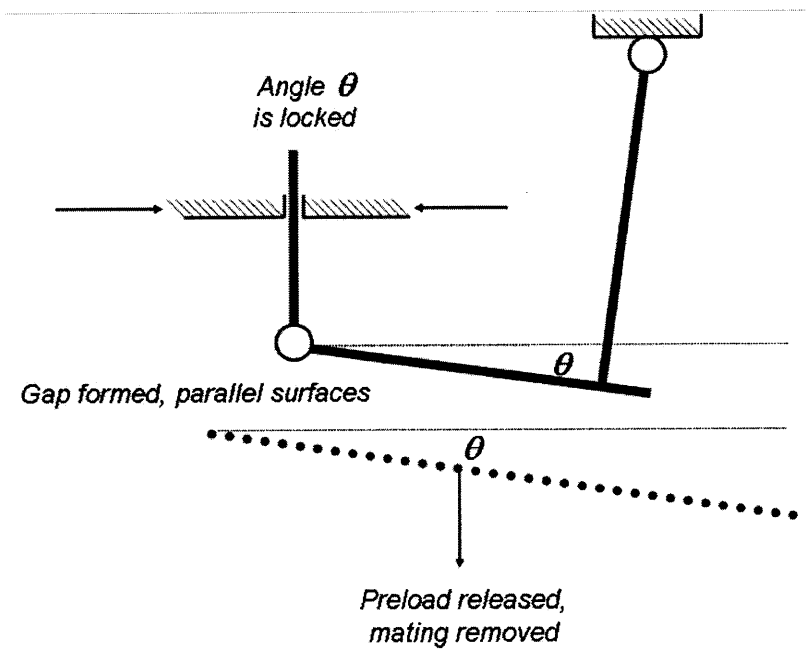
Figure 2-12: Preload released and gap formed with ideally parallel surfaces

33

2.7 Compliances and Stiffnesses

This section describes aspects of the design which were decided based on simulations and given constraints. With the architecture of the system in place, we needed to determine the dimensions of the flexural elements.

The axial stiffness of one double parallelogram was given by Equation B.4. With our design, we had two double parallelograms, one on each side, making the stiffnesses act in parallel. This is given by Equation 2.3.

$$k_{parallel} = 2k_y = \frac{24EI}{L^3} \tag{2.3}$$

In order to derive the rotational stiffness of the two double parallelograms in parallel, we did a simple moment balance on the system. This is shown in Appendix B. The result is Equation 2.4

$$k_{\theta,top} = 2k_y r^2 \tag{2.4}$$

We used two double parallelograms in parallel, in both the top and bottom modules. With a stiffness given by the following equation, the overall axial stiffness of the double parallelogram system was twice as much. Figure B-8 shows the derivation for the rotational stiffness for two double parallelograms in parallel. In the top and bottom module there is a pair of double parallelograms.

Figure B-6 in Appendix B states the stiffnesses of the various components. In short, the axial stiffness of the bottom parallelogram is 6 times more stiff while the rotational stiffness is 100 times more stiff.

2.8 Error Analysis

This section describes the error analysis done to see the various sources of error. Ideally, after the preload in the bottom module is released, the angle formed from conformal contact is expected to stay fixed. However, various effects could change this angle and were considered in the error analysis.

2.8.1 Uncertainty in Angle

2.8.2 Temperature Variation

Variation in temperature in space and time could affect the measurement. First, the sensors can be sensitive to this change. Second, depending on the coefficient of thermal expansion for the material of the system, additional displacement could occur. This can in turn change the angle of the top module. This is given by Equation B.2

$$\Delta l = \alpha \Delta T l_0 \tag{2.5}$$

where α is the coefficient of thermal expansion and δT is the variation in temperature, l is the deformed length and l_0 is the initial length.

2.8.3 Hinge Effect

As the top module is being forced into compliance to the bottom module, elastic energy is stored throughout the elements. An input torque and angular displacement is caused by the bottom module. The preload prevents the bottom module from applying the restoring torque. Therefore, once the preload is released, the top module will want to go back to its original state. If the mechanical clamping of the post is not ideal, then there will be a change in angle.

2.8.4 Poisson's Ratio

As the post is fixed on both sides, the stress from the clamping will cause the post to have strain in the orthogonal direction. Analysis from ABAQUS was done to model the contact mechanics between the clamp and the post. In Fig. 2-13 and Fig. 2-14 are the Solidworks model and ABAQUS analysis results of the study. In Figure B-7 are the summary of the simulations, showing a range from 450-800 nm displacement. For the specific model showed in Figure 2-14, the displacement was on the order of 570 nm. Appendix B.2 shows two additional pictures, Figure B-1 and B-2 that show

the 200 N being applied and the mesh of the model. Across a lever arm of about 2.5 inches, this results in a change of angle on the order of 10 μrad. For the error analysis conducted in Chapter 4, an approximate value of 1000 nm or 1 μm was used.
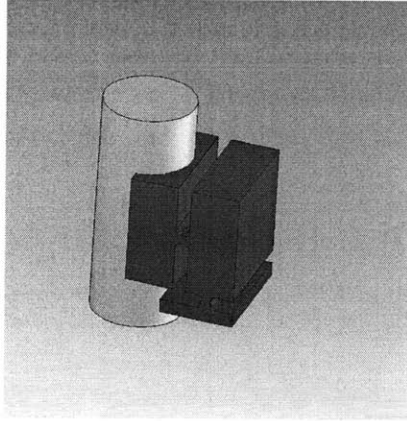
Figure 2-13: Solidmodel of in-plane clamp modeled in Solidworks

2.9   Summary

This chapter covered the design used for this study. After considering previous work, we decided to use flexural elements to meet the functional requirements of our setup. Simulations were done to find the best dimensions of the system.

U, Magnitude
+7.891e-03
+7.234e-03
+6.576e-03
+5.919e-03
+5.261e-03
+4.603e-03
+3.946e-03
+3.288e-03
+2.630e-03
+1.973e-03
+1.315e-03
+6.576e-04
+0.000e+00
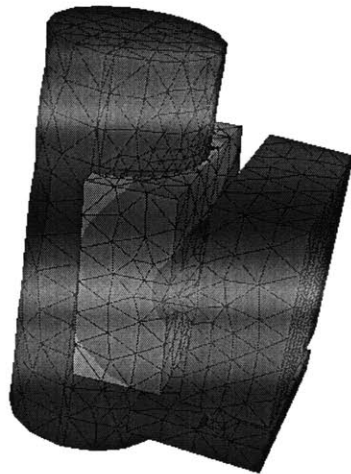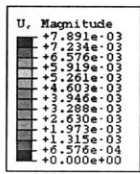
ODB: inplane_20_170-2.odb   ABAQUS/STANDARD Version 6.6-3   Mon Apr 02 15:12:25 Eastern Daylight Time 2007

Step: Release, Release
Increment   1: Step Time =   1.000
Primary Var: U, Magnitude
Deformed Var: U   Deformation Scale Factor: +7.319e+02

Figure 2-14: Post-processing results of ABAQUS simulation. See Figure B-1 in Appendix B.2 for application of load

THIS PAGE INTENTIONALLY LEFT BLANK

Chapter 3

Manufacturing

3.1 Introduction

This chapter looks at the manufacturing and assembly considerations taken in the development of the planar mechanism. With restraints of cost and time, tradeoffs were made in order to achieve the best instrumentation for the desired goals.

3.2 Design for Manufacturing

This section discusses the final decisions made on key components of the design, when considering manufacturing.

3.2.1 Post

Ideally, the post would be lathed and threaded out of cylindrical stock. Then, it would be assembled onto the top surface. This cylindrical geometry would be similar to a capacitance probe being held in the in-plane clamp. However, for this study, we decided to make the post as part of the monolithic top module. Although this would limit the types of post possible, this would simplify machining steps and assembly.

With this change, we had to consider what sort of mating geometry we could make with a monolithic structure. Shown in Figure 3-1 below is the final design. Although

this is not the exact same geometry as was in the ABAQUS analysis, the dimensions are on the same scale.
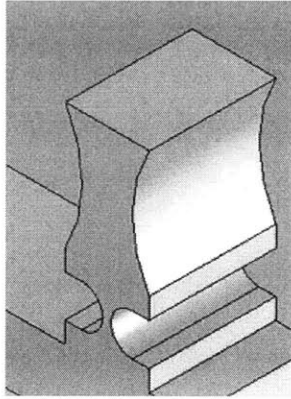
Figure 3-1: Solidmodel of post

3.2.2   In-Plane Clamp

The in-plane clamp was decided to be a separate module from the top module. This would allow future work to investigate variations in dimensions and geometry for the in-plane clamp, if certain designs could not sufficiently clamp the post. The clamp matched the shape of the post. The centers of the circle, with same radii, were shifted by a small distance. This shift was shown in Figure 3-2 shows the sketch from Solidworks in offsetting the circle to create matching shapes.

3.2.3   Mounting Components

For the sensors and actuators, adapter plates were designed to hold mounts for the micrometers and capacitance probes. The adapter plates conformed to the 1" spacing on the optical breadboard while having appropriately spaced threaded holes for the housing. This modular approach allowed for ease of debugging during the experiments.
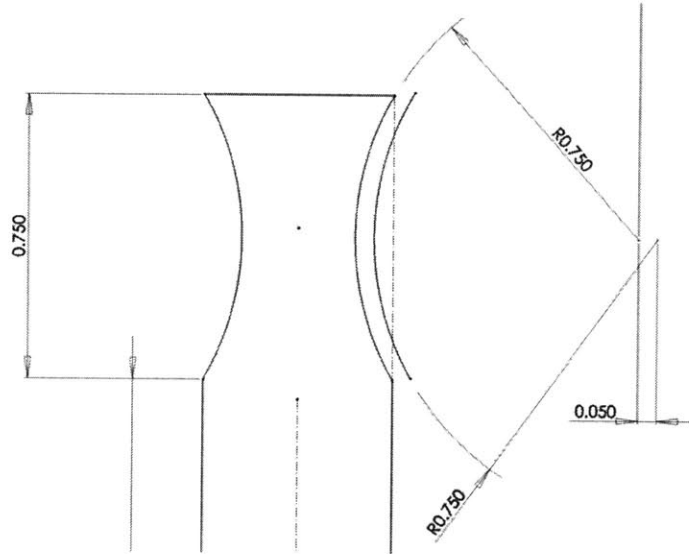
Figure 3-2: Sketch of offset circles

3.3 Manufacturing

This section looks at the considerations that were made for design for manufacturing and assembly: materials, machining methods, and system architecture.

3.3.1 Orientation of Instrumentation

In actual uses of the small-scale gaps, such as the filtration of biologically active molecules, the instrumentation would need to be in a vertical orientation. To ease machining and assembly, we decided to orient the planar mechanism horizontally, with gravity acting in and out of the plane of motion. This helped with the design as we could use an optical breadboard, as shown in here, to mechanically ground the elements. Figure 3-3 illustrates one of the designs that had gravity acting in the direction of actuation and motion.

3.3.2 Choice of Materials

After considering machineability and ease of access and cost, Aluminum 6061 was chosen for the material to fabricate the parts. This material was purchased from the
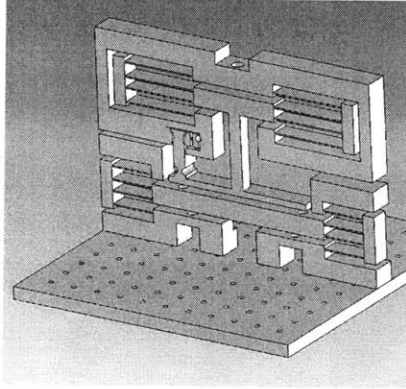
Figure 3-3: Earlier design which was mounted vertically

MIT Central Machine Shop and also used extra materials from the MIT Hobby Shop.

3.3.3 Choice of Manufacturing

The flexures designed in the previous chapter can be easily manufactured by means of abrasive waterjet technology or wire electro-discharge machining (EDM) [13]. Although wire EDM provides a better resolution and better surface machining, the waterjet is relatively economical compared to wire EDM. Also, it was easier to access.

3.3.4 Integral and Modular Design

We desired for our system to have both integral and modular aspects to the design. The top and bottom module was desired to be machined as a monolithic structure, to reduce assembly and interface issues. Although this limited our design, we were able to focus on the in-plane clamp. The top and bottom modules were also designed to be reusable for future experiments since the cost on the waterjet was relatively expensive.

However, we also wanted modular aspects of the design to allow for future experiments with the existing hardware. Since the focus of the study is to investigate the peformance of in-plane clamping, this system architecture allows for additional in-plane clamps to be designed.

3.4 Fabrication

This section describes the machining processes that were done to create the mechanism. Many lessons were learned for future instances of manufacturing.

3.4.1 Waterjet

The OMAX waterjet machine at the MIT Hobby Shop was used for the flexures and quickly making other parts. For example, the top module shown in Figure 3-4 here took 2 hours of waterjet time to make. After the design was modeled in Solidworks, it was saved as a drawing exchange file (.DXF). OMAX Make was used to plan out the path of the waterjet nozzle. Figure 3-5 is a picture of the OMAX waterjet machine in the MIT Hobby shop.
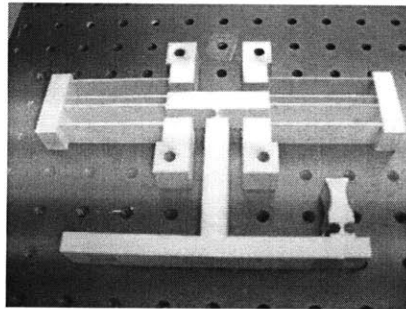
Figure 3-4: Top module – took approximately 2 hours to waterjet

Figure 3-5: OMAX 2626 JetMachining Center in MIT Hobby Shop

The actual cutting path of the part always needed to have an offset from the stock, so that the resulting piece would be cut cleanly. Also, it was suggested that

conventional machining be done after waterjet, instead beforehand. With one of the test in-plane clamps, we had machined first, then waterjet. In Fig blank Since care was not taken to precisely align the machined piece to the waterjet nozzle, the misalignment caused a failure in the in-plane clamp, as shown below. Figure 3-6
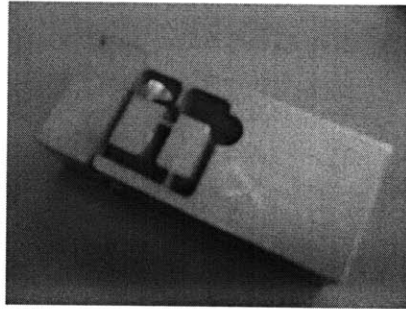
Figure 3-6: In-plane clamp failed in waterjet step because of misalignment

A disadvantage to waterjetting is the taper that is caused as the nozzle pierces into the thickness of the material. Figure 3-7 illustrates one type of taper, called a "v-shaped" taper, where the top of the cut is wider than the bottom. This occurs because the jet spends more time piercing through the top than the bottom, allowing more area to erode at the top [14].
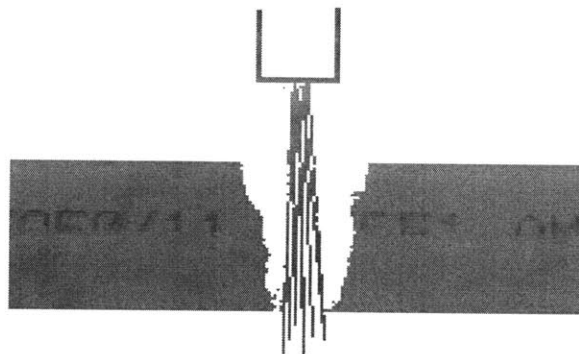
Figure 3-7: Illustration of "v-shaped" taper, where top of cut is wider than the bottom. Courtesy of OMAX [14]

After getting a test cut, it was found to be a varation of 0.01" along the depth of the cut. We decided that this was acceptable for our purposes. For the mating of the top and bottom surfaces, however, this would present a problem. The solution to this

was to flip the bottom module in order for the tapers to made better. This avoided a delicate post-machining step of facing off the surface. Figure 3-8 shows 3/4" stock aluminum after components have been waterjet.
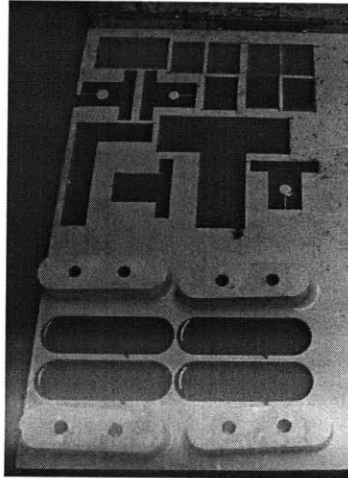
Figure 3-8: 3/4" spacers after waterjet. Above that are other components

3.4.2 Conventional Machining

There were instances when there were machining steps that could not be done on the waterjet. For instance, each of the individual housing pieces for all the components was first cut on the waterjet. This created the hole in which the components sat and the split clamp. Holes for the pieces were undersized on the waterjet and reamed out to dimension afterwards. Then, they needed two sets of machining steps: one for the set screw for the split clamp and another for the mounting holes to the adapter plate. The set screw tightened the fit between the component and hole. These cuts were in different directions and therefore needed conventional machining.

The bottom module needed to have through holes for the capacitance probe. Wooden shims were created to prevent the blades from vibrating during machining. Figure 3-9 shows the setup needed for the bottom flexure while we machined it. The mounts for the micrometers and capacitance probes also needed shims for drilling through holes and tapping. Fig 3-10 and 3-11 shows additional components.
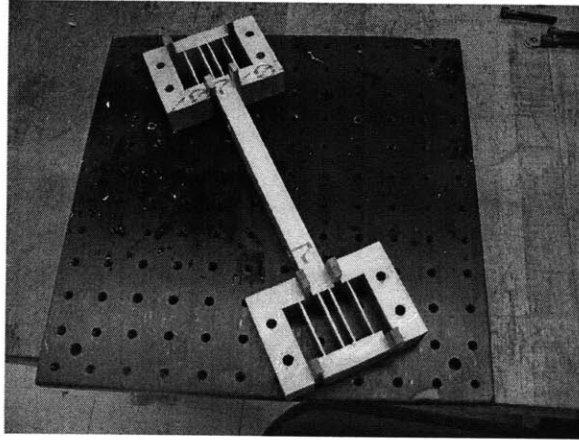
Figure 3-9: Wooden shims placed to prevent flexing
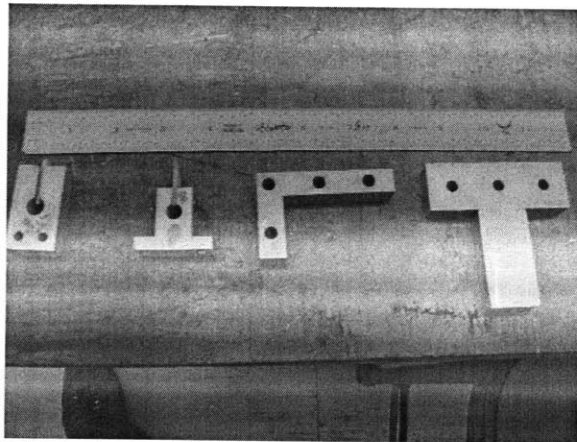
Figure 3-10: Additional post-waterjet machining

3.5 Summary

In this chapter, the account of manufacturing and machining was recalled. There were many practical lessons learned that would not have been gained from considering the solidmodel or simulations.
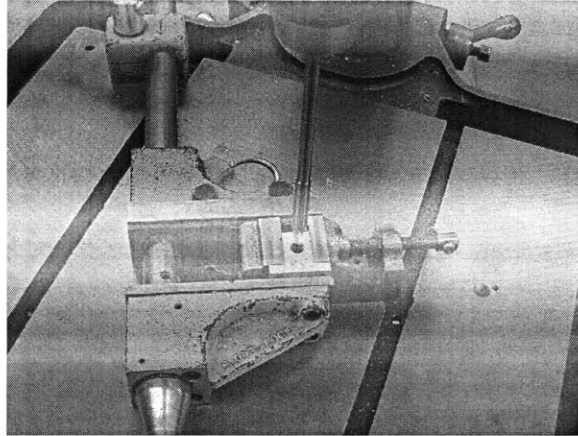
Figure 3-11: Reaming a 9.5mm hole for holding, done at MIT Edgerton Student Shop

THIS PAGE INTENTIONALLY LEFT BLANK

Chapter 4

Experiments

4.1 Introduction

This chapter describes the hardware and the procedure for the experiments, along with the experimental results.

4.2 Hardware

This section describes the sensors and actuators used in the setup, along with other pieces of hardware.

Two Mitutoyo 148-132 micrometer heads were used for positioning the two modules. These components also provided the preload. A split clamp was used to hold the micrometers in place. Both micrometer heads had a range of 0-13 mm and a resolution of 10 μm.

ADE 2805 capacitance probes were used, along with the corresponding 3800 modules. They were factory calibrated against a laser interferometer.

The capacitance probe modules needed to be powered by $\pm$ 15 V. The probes were rated to have a resolution on the order of 2 nm, with the analog module set to a cutoff frequency of 100 Hz. The actual use of the probes required them to be brought within a standoff distance of 75-125 μm. This corresponded to an output voltage of $\pm$ 10 V. Additionally, the target of the capacitance probe needed to be grounded to

the chassis of the probe module.

We decided to decouple the mounting of the capacitance probes to either of the two modules. This meant that the capacitance probes were always fixed to ground. They only measured the change in angle of the top flat and the measurement would not change with any motion in the bottom flat. Further, we needed to handle the capacitance probes carefully, as electro-static discharge could damage the probes. Also, they could not be clamped too tightly or else the shell would fracture.

A 12" by 12" aluminum optical breadboard from Thorlabs was used as a mechanical ground for the whole assembly. The breadboard was fixed to a vibration isolation table.

4.3 Assembly

This section describes putting together the parts after machining along with wiring electronic instrumentation.

4.3.1 Assembly of Parts

The flexures were handled with care as the parts were assembled. While assembling and reassembling the system many times, we realized that it was good that many aspects of the design were modular.

4.3.2 Wiring of Instrumentation

After the mechanical assembly was fastened together, the appropriate electrical connections were made. The output voltages from the capacitance probe modules were recorded using a HP 34401 multimeter. A handheld multimeter was used to debug connections before powering on the system.

4.4 Experimental Procedure

Figure 4-1 shows the experimental setup.
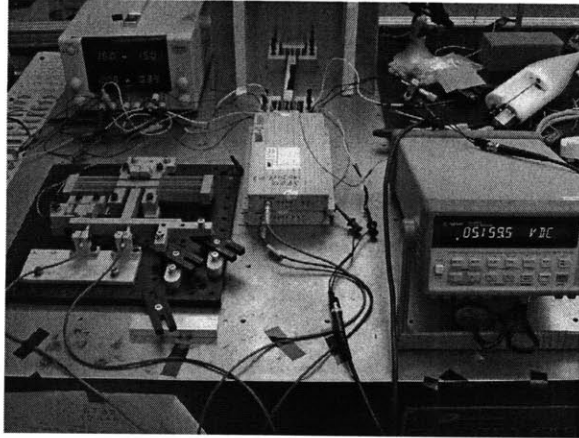
Figure 4-1: Experimental setup, modified slightly from original design. Explained in Section 4.6

4.4.1 Capacitance Probe Check

Before running the experiments, we wanted to make sure that the capacitance probes worked properly. We did this by only using the top module and the micrometer head at the top to displace the top surface. The micrometer head was moved between to distances of 20 μm, according to the count on the micrometer head.

Figure 4-2 shows the distance traveled on both sides, according to the capacitance probes. It shows that the capacitance probe accurately measured the distance traveled, within the resolution of the micromter.

According to the micrometer head, 20 μm were displaced and the sensors indicated a motion of about 15 μm. This is reasonable since the resolution of the micrometer head was 10 μm. Further, backlash and human error in the measurements could account for the deviation. There were some occasions in which target fell too far or too close to the capacitance probe. This was either from backlash of the adjustment of the micrometer head or the relatively rough finish of the waterjet cut. This explains the circled points in Figure 4-2 that are at 55 55 μm. The remaining data points indicate that the capacitance probes worked properly.
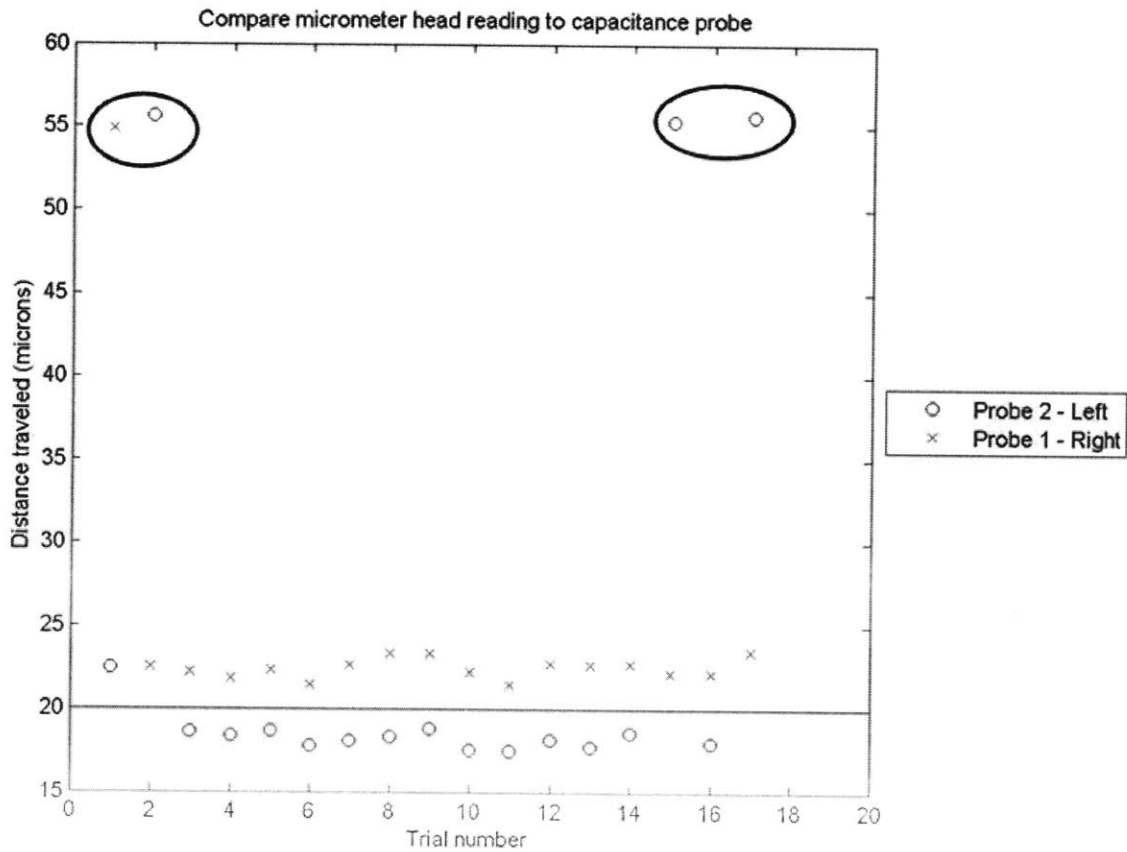
Figure 4-2: Distance traveled according to capacitance probe. Shows that capacitance probes were measuring correctly. Readings that were out of range are circled. This might have been caused by backlash in the adjustment of the micrometer head, possibly putting the target out of range.

4.4.2 Conformal Contact and Locking of Post

First, the top micrometer head was turned to displace the top module flexure enough to make contact, creating a preload at the top. Next, the bottom micrometer head was turned to displace the bottom module to make contact with the top module. There was an initial misalignment of angle because of the bolting, but this was acceptable as it gave a clear initial misalignment. Once it was felt that the bottom micrometer could push no longer, a 1/16" NPT pipe plug was turned into its hole, clamping the post to fix the position. The height of the central beam and the rigid post were then fixed. Therefore, the angle was set.

Figure 4-3 shows the pipe plug being tightened in order to force the flexure to clamp the post.
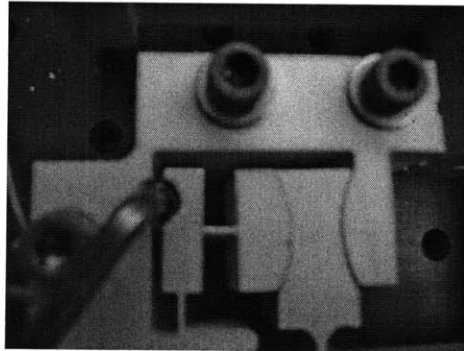
Figure 4-3: A hex key tightens the pipe plug, causing the flexure to bend and clamp the post

4.4.3 Standoff Distance for Capacitance Probes

Next, the capacitance probes were brought within the near and far standoff distances of 75 and 125 μm respectively. Figure 4-4 is a diagram of the capacitance probe and the standoff distances with respect to the target.

Each probe had a range of 50 μm. Only within this range threshold give output voltages. Therefore, we needed to adjust the position of the cap probes by hand, before starting the experiments. Once they were within standoff distance, the set screw was tightened to hold it in place. The wires were all strain relieved to isolate any disturbance motion. Once probes were within the measurable range, a reading was recorded.

4.4.4 Release of Preload

Next, the preload of the conformal contact applied on the bottom module was released by backing out the bottom micrometer. With the preload at the bottom removed, the top flexure would want to spring back. Bringing back the bottom module simulated the formation of the gap. A second reading was recorded after the bottom preload was released.
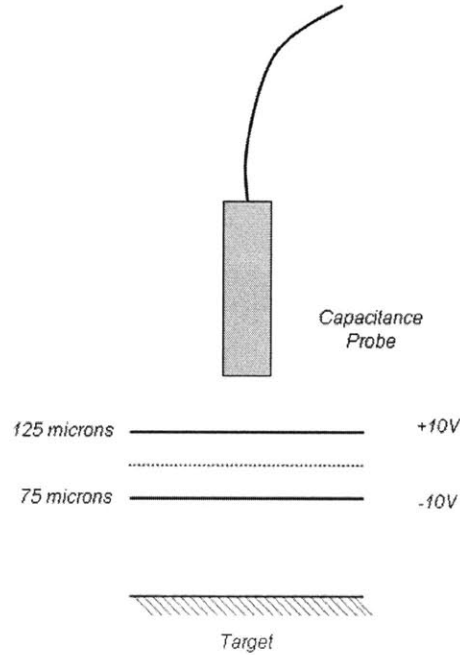
Figure 4-4: The capacitance probe must lie between the 75 and 125 μm standoff distances. Here the probe is outside the far standoff distance.

4.5 Initial Results

Shown in Figure 4-5 are the readings of capacitance probes as the preload is being released. This indicated that the top surface was moving at least 50 μm, signifying that the clamping force applied on the post was insufficient.

4.6 Procedural Adjustment

This section describes the modification to the setup and experimental procedure after the inital experiments.

4.6.1 Waterjet Taper

From previous test pieces, we knew that matching the tapers would help with the clamping. However, through the initial tests, we realized that this was critical for the clamping of the system. Figure 4-6 and 4-7 illustrate the matching and mismatching
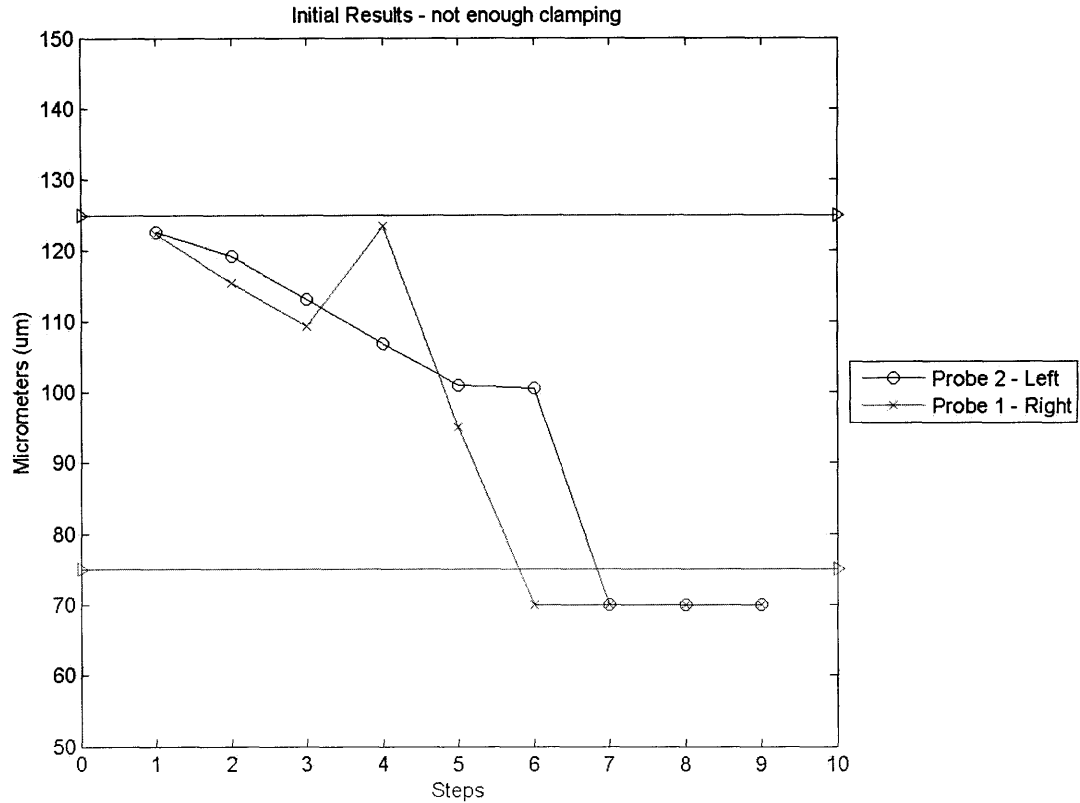
Figure 4-5: The measurements indicate that the clamping was not sufficient

of the taper from the waterjet.

4.6.2 Modification to Setup

We realized that the tapers were not matched, as shown in the figure below. We thought that there would be sufficient contact for clamping. However, this was not the case. Also, since the assembly was not designed for the rearrangement to match tapers, we had to take out the bottom module. Due to time constraints, we could not re-machine the bottom module or any of the components in order for the system to work as designed. However, we were able to apply a preload using clamps from the optical breadboard system. We rearranged the components and came up with the following setup in Figure 4-8:

Figure 4-9 shows an improvised setup to create a preload force. Unlike the microm-

Tapers mismatched
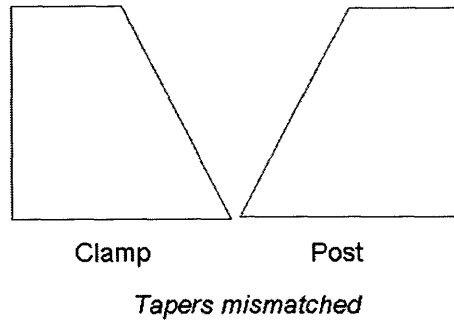
Figure 4-6: The original configuration. Lack of contact prevented proper clamping of the post

Tapers matched to mate
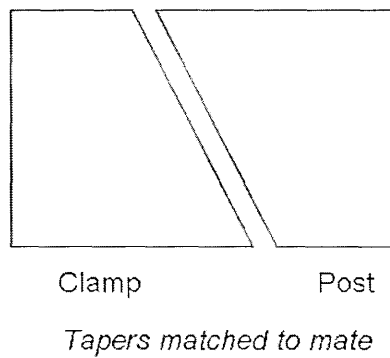
Figure 4-7: When the waterjet parts are reversed, the tapers can match, for proper contact for clamping

eter head, it could not step down the force incrementally. However, it still provided the preload we needed to hold the angle before the clamp was locked. It was released by loosening one of the bolts.

4.7 Results

This section discusses the results and draws conclusions from the data.

4.7.1 Processing of Data

Two measurements were recorded for the position of the top surface with the capacitance probes. The first measurement was recorded after the post was locked. The
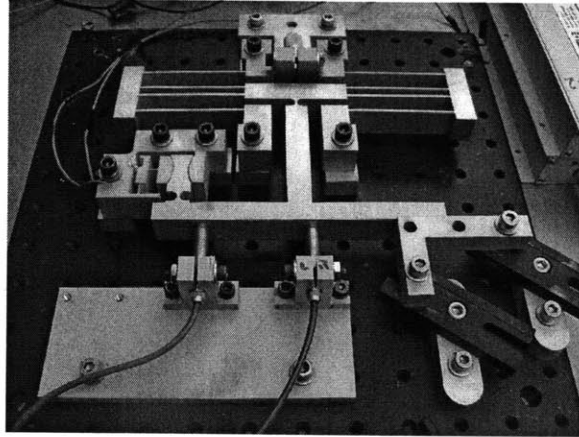
Figure 4-8: Modified setup with tapers matched between clamp and post. Preload from bottom right
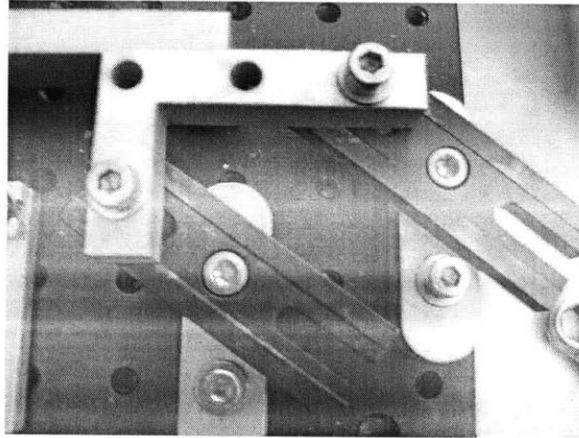
Figure 4-9: Close-up of the preload force that was created because the bottom module could no longer fit

second reading was recorded after the preload was released, with the post locked. In the 10 trials that were attempted, four were successful. The highest uncertainty in angle was on the order of 50 μrad, for the latter. Figure 4-10 shows the results from the 4 trials and the change in angle, i.e. the resultant uncertainty in angle.

In the unsuccessful trials, the displacements measured by the capacitance probes often were outside the range of 50 μm. First, the clamping force on the post may not have been sufficient to hold the post in place. This meant that the angle was not held. Once the preload was released, the top surface went back to its original

position.

Second, the surface finish of the target was from the waterjet cut. For future work, the part will be planned out to make sure that both mating surfaces have a smooth finish. The roughness of the waterjet cut limited the close range measurement of the capacitance probes.

Future work will focus on investigating the possible sources of error for the next set of trials, in order to check the repeatability of the current results. The detailed steps are presented in Section 5.2
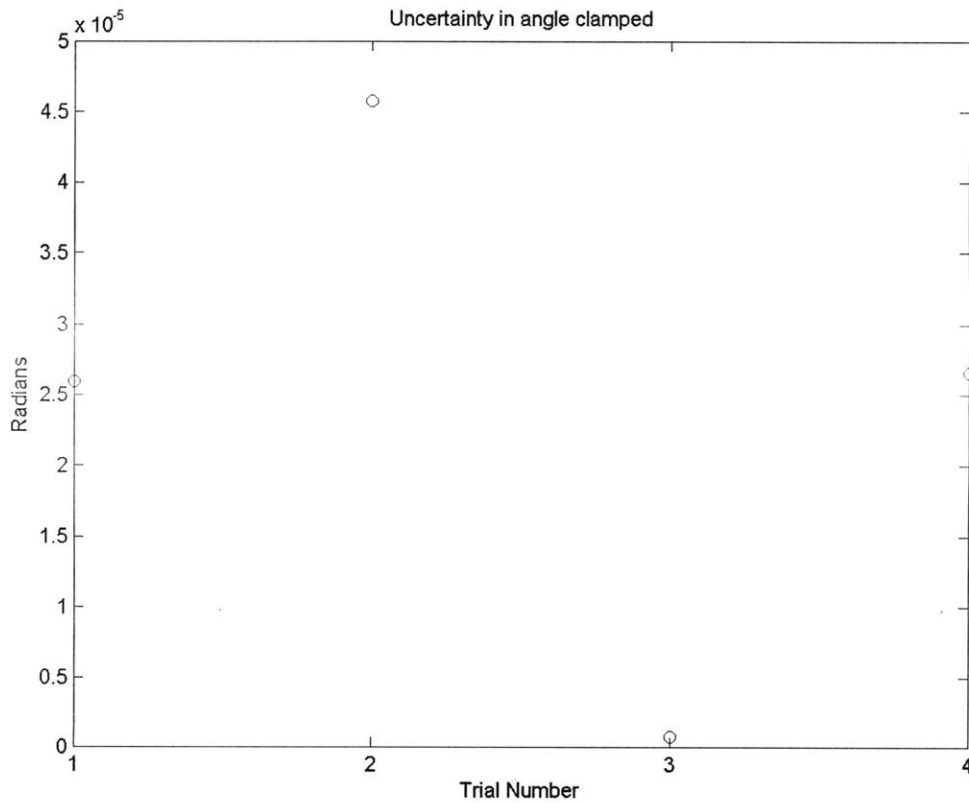
Figure 4-10: Highest uncertainty in clamped angle was 50 μrad

4.7.2 Error Analysis

Based on error analysis described in Chapter 2, we calculated the theoretical uncertainty in alignment for the design we used in the experiments. Figure 4-11 shows the

different heights. The surface which is length L will change in angle depending on the factors mentioned earlier: temperature, springback, Poisson's ratio. The analysis is based on the Equation (B.1)

$$\delta\theta = \frac{\delta h_1 + \delta h_2}{L_{between}} \tag{4.1}$$
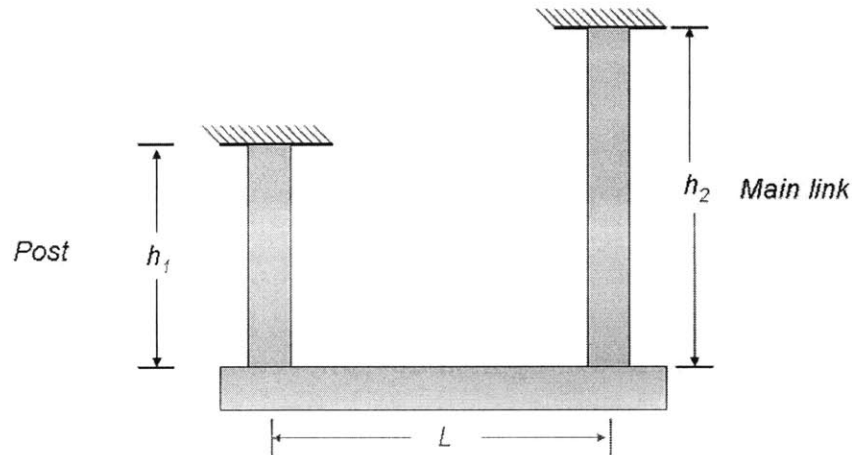
Figure 4-11: Diagram of the error analysis, with two heights and the angle formed by the surface joining the two

Figure B-3 shows the predicted uncertainty. Appendix B shows the other calculations. The uncertainty was on the order of 50 μrad which matches with the range of experimental data. The lever arm between the main link and the post could be increased to reduce alignment error.

4.8 Summary

In this chapter, the experimental procedure was discussed, from the assembly of the parts to the experimentation. We found that clamping errors result in an uncertainty in alignment, on the order of 50 μrad which agrees with the error analysis performed.

THIS PAGE INTENTIONALLY LEFT BLANK

Chapter 5

Conclusions and Recommendations

5.1 Summary of Work

In this section, we detail the contributions in terms of design, manufacturing, and testing and instrumentation, for the area of programmable small-scale gaps. The most practical outcome of this work is the assembly of a functional hardware setup that can be used for further characterization and experiments.

5.1.1 Design

Based on previous work done in programmable small-scale gaps, we examined a new way to lock the angle once conformal contact was made. This approach is advantageous because once the alignment is made, the control system only needs to control the gap height. We selected flexural elements such as the double-parallelogram, in-plane clamp, and notch flexure to produce the smooth motion asrequired.

5.1.2 Manufacturing

After designing the system, we used abrasive waterjet technology to manufacture the flexural elements. We learned many lessons about limitations of this process. The taper that the waterjet taper was critical in the design. Also, the finish of the surfaces will affect the readings from the instrumentation.

5.1.3 Instrumentation and Testing

We used micrometer heads and capacitance probes. Through testing, we realized the difficulty in bringing the capacitance probes within standoff by hand. Considering the trials in which the post was clamped sufficiently, leading to measurable change, the highest uncertainty in angle was 50μrad. This makes the concept presented appropriate to micro-scale applications, but limits its use for nano-scale alignments.

5.2 Future Work

In this section, we discuss the plans for the next iteration of the planar mechanism.

5.2.1 Design

We desire to take a more rigorous look at the mechanics of the in-plane clamp. The dynamics of this flexural element need to be more thoroughly understood in order to optimize the design. Eventually, the next step should be to take this idea to a three-dimensional application, with control of the three rotational degrees-of-freedom.

5.2.2 Manufacturing

For future work, the in-plane clamp should be re-waterjeted so that the tapers match, ensuring conformal contact between the clamp and post. Also, wire EDM could be considered as a manufacturing option. Insert figure with future solidmodel picture. Also, the surface of the target needs to be machined to a fine finish, so that we are not limited in the range of our capacitance probes.

5.2.3 Instrumentation and Testing

For bringing the capacitance probes, flexures should be made and a micrometer head should be added for each probe so that it can be positioned within standoff distance easily and repeatably, at a high resolution. This is shown in Figure 5-1
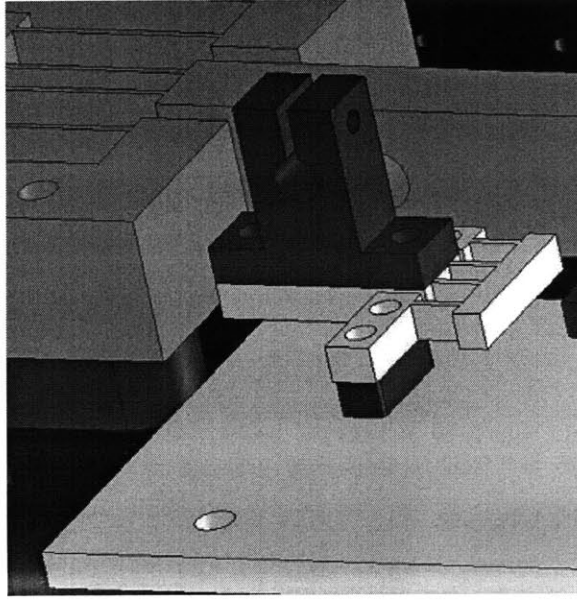
Figure 5-1: New flexures to be machined and added to the assembly to allow for fine manual control of capacitance probes

In order to investigate the transient behavior of the top surface, the probe modules would be hooked up to dSPACE environment to allow for easier acquisition of data. Also, eventually closed-loop control should be implemented in order to actively control the height gap once alignment is made. This would involve the use of a piezoelectric actuator and another capacitance probe for sensing the gap height.

THIS PAGE INTENTIONALLY LEFT BLANK

Appendix A

Design Alternatives

A.1 Introduction

This appendix will provide designs during this process which were considered but not chosen as the final design.

A.2 Design 1

This was an initial design that was meant to be completely monolithic. The problems that came with this design were realized once we considered manufacturing and assembly considerations. The micrometer heads modeled in the picture would be hard to reach to adjust. There would need to be a way to clamp the micrometer head. Fig. A-1 is a solid model of this design. At that point, we did not calculate how long it would take to waterjet such a structure. Having spent a lot of time on the waterjet in hindsight, this would have taken many hours on the waterjet, and the slightest disruption in machining would have affected the whole piece.

A.3 Design 2

This next design was not used because there needed to be an additional component for rotational compliance. The top module would have been preloaded by the micrometer
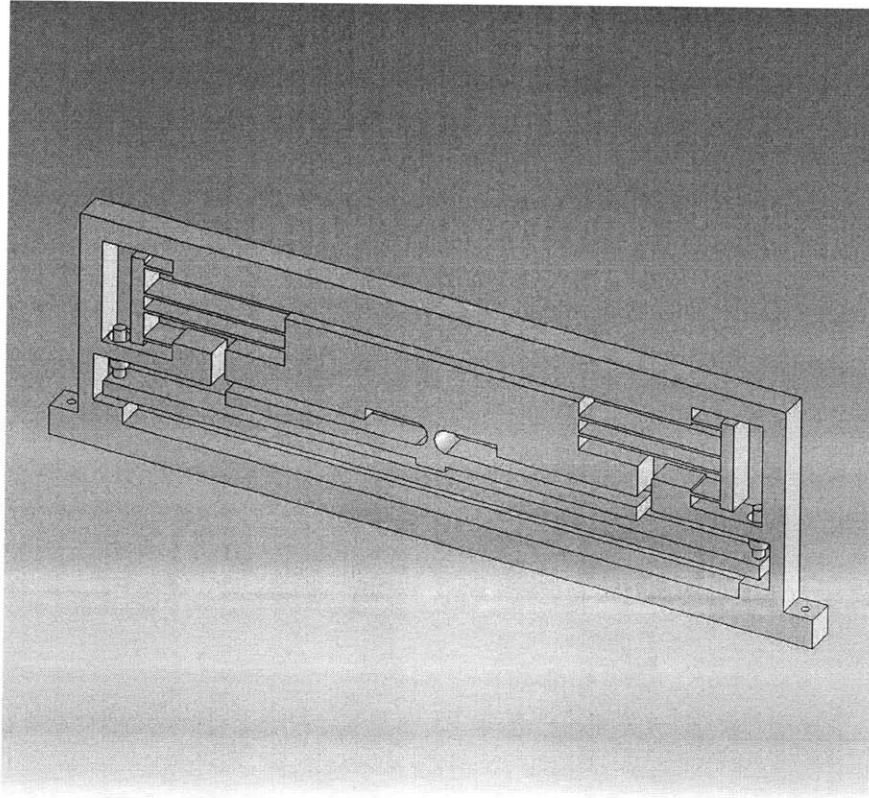
Figure A-1: Initial completely monolithic design

head or piezoelectric actuator. With this, the double parallelogram at the top would be rotationally stiff. Therefore, a notch flexure was added between the main link and the main stage of the top parallelogram to provide rotational compliance. Figure A-2 shows this design. In blue is the micrometer head and in red are the capacitance probes.
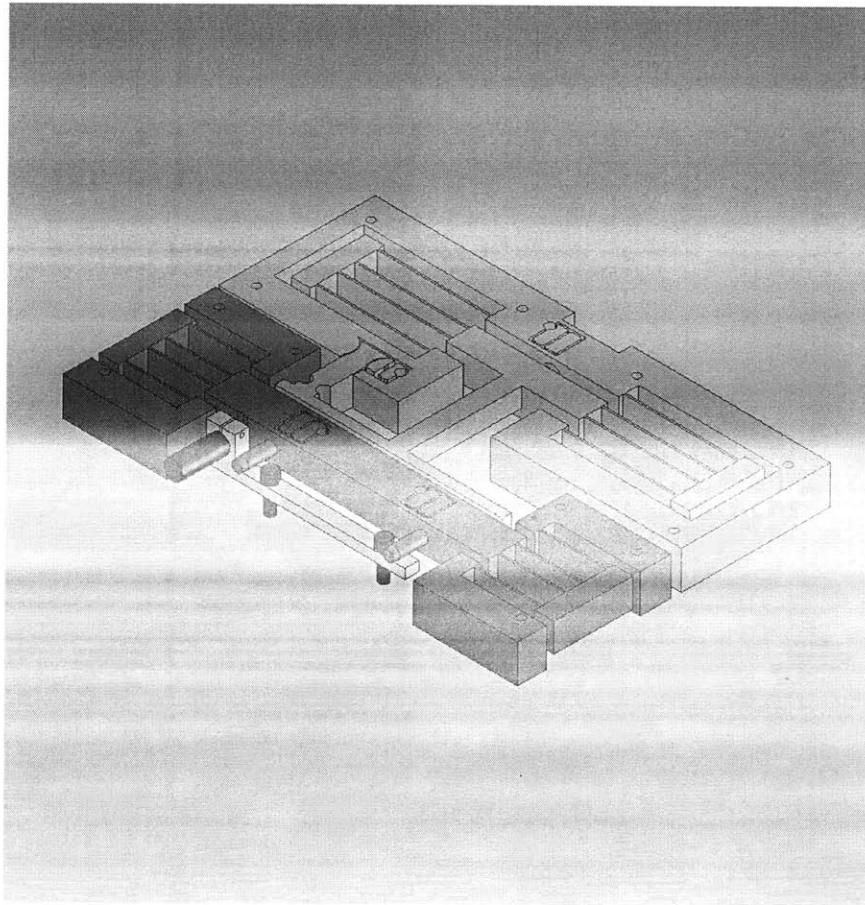
Figure A-2: Rotational flexure needed. Blue - micrometer head. Red - capacitance probes

Appendix B

Additional Figures

B.1 Introduction

This appendix will provide additional data, derivations, code, and figures.

B.2 Extra Figures
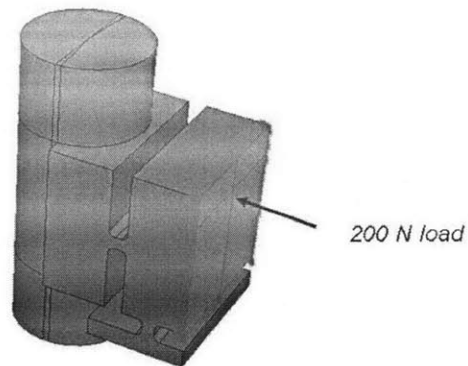
Figure B-1: ABAQUS model referred to in Section 2.8.4, with load of 200 N shown
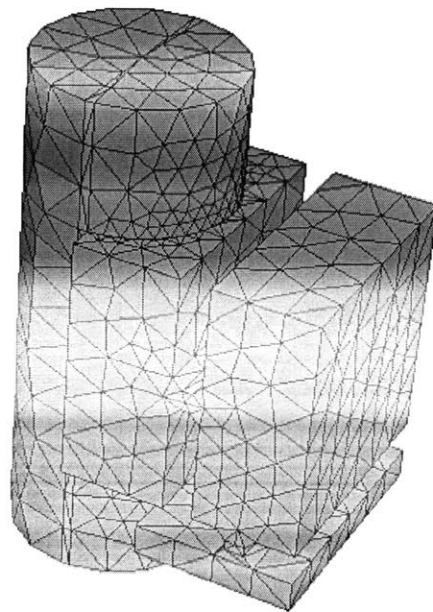
Figure B-2: ABAQUS model referred to in Section 2.8.4, with mesh shown

B.3   Spreadsheets

Effect	Delta h1 (post)	Delta h2 (main)	Delta Theta		Distance between the two	2.5 in
						0.0635 m
Springback			2.29E-06			
Temperature	2.92E-07	1.61E-06	2.99E-05			
Poisson's ratio from clamping	1.00E-06	0	1.57E-05			
		Total	4.79E-05			
			48 microradians			

Figure B-3: Contributions of uncertainty from temperature, Poisson and springback effects

The following equations were used in spreadsheet B-3 for Figure B-4.
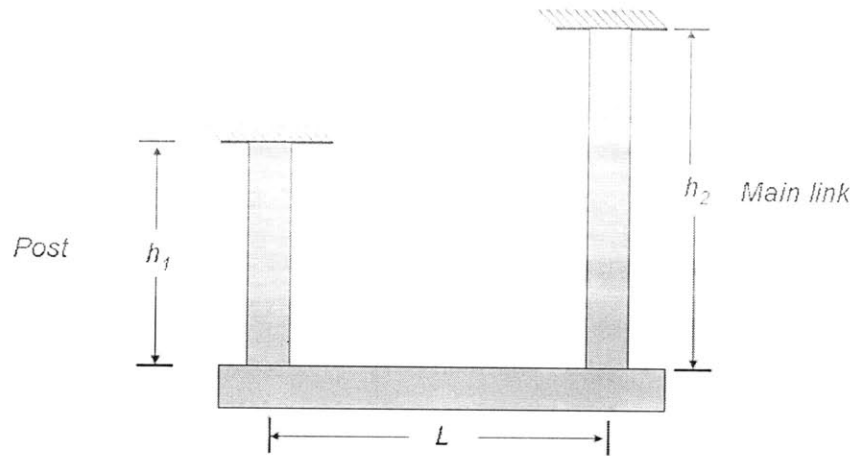
Figure B-4: Diagram of the error analysis, with two heights and the angle formed by the surface joining the two

$$\delta\theta = \frac{\delta h_1 + \delta h_2}{L_{between}} \tag{B.1}$$

$$\Delta l = \alpha \Delta T l_0 \tag{B.2}$$

71

$$\theta_{springback} = \frac{k_{notch1,rot}k_{notch2,rot}\theta_{error}}{k_{main,ax}l_1^2 + k_{post,ax}l_2^2} \qquad (B.3)$$

Change in temperature	1	C		
Coefficient of Thermal Expansion	2.30E-05	per C		
Distance between two heights	2.50E+00	in		
	6.35E-02	m		
	height (in)	height (m)	delta from temp	
h1 (post)	0.5	0.0127	2.92E-07	
h2(main)	2.75	0.06985	1.61E-06	
		sum	1.90E-06	
		divided by the length in betewen	2.99E-05	Theta error

Figure B-5: Contributions of uncertainty from temperature

Spreadsheet B-6 uses the following equations:

$$k_y = \frac{12EI}{L^3} \qquad (B.4)$$

$$k_{parallel} = 2k_y = \frac{24EI}{L^3} \qquad (B.5)$$

$$k_{\theta,top} = 2k_y r^2 \qquad (B.6)$$

Young's Modulus Al	7.00E+10	Pa		
Top module thickness	0.75	in		
	0.01905	m		
Bottom module thickness	1	in		
	0.0254	m		

Double parallelogram		thickness (in)	thickness (m)	blade length	blade length (m)	blade thickness	blade thickness (m)	I-moment of inertia	Axial stiffness of one double parallel (N/m)	Main length (in)	Main length (m)	R = M.S length/2 (m)	Rotational stiffness of module
	top module	0.75	0.01905	2.5	0.0635	0.05	0.00127	3.25161E-12	1.07E+04	2.4	0.06096	0.03048	1.98E+01
	bottom module	1	0.0254	1.5	0.0381	0.05	0.00127	4.33574E-12	6.59E+04	7.5	0.1905	0.09525	1.19E+03

Notch flexure		thickness (in)	thickness (m)	radius of arc (in)	radius of arc (m)	centers distance (in)	centers distance (m)	centers thickness (m)	Rotational stiffness of notch (N-m)	Axial stiffness of notch (N/m)	Effective area (m²)	Effective length, or height of notch (in)	Effective length, or height of notch (m)
	Main	0.75	0.01905	0.125	0.003175	0.3	0.00762	0.00127	9.62E+01	2.67E+08	2.41935E-05	0.25	0.00635
	Post	0.75	0.01905	0.125	0.003175	0.3	0.00762	0.00127	9.62E+01	2.67E+08	2.41935E-05	0.25	0.00635

	b (in)	b(m)	h(in)	h(m)	L(in)	L(m)	A(area)		Axial stiffness	
Main link axial	0.75	0.01905	0.5	0.0127	2.75	0.06985	2.4194E-04		2.4245E+08 Two in series	
Notch post axial	0.75	0.01905	0.5	0.0127	0.125	0.003175	2.4194E-04		5.3340E+09	2.6670E+09

Axial stiffnesses		Distance to pivot (m)	Distance to pivot (in)
Main	1.2700E+08	0.0635	2.5
Post	2.4245E+08	0.12065	4.75

Initial misalignment	1.00E-03
Angular Uncertainty	2.2906E-06

73

Justin Lai 4/2/2007

Chord Length	19.92 mm	
L_clamp	24 mm	diameter - diameter of post
L_ends	12.5 mm	alpha - total angle of arc length of surface contact
L_total	49 mm	theta_star - degrees of rotation of partition plane
Thickness of assembly	25 mm	(180-alpha)/2 = theta_star
		26mm*sin(100degrees/2)

mirrored contact areas

theta_star	diameter (mm)	alpha	Top displacement	Bottom Displacement (mm)	Bottom Displacement (nm)
	19	180.00	4.436E-04	4.527E-04	453
5.22	20	169.57	5.704E-04	5.679E-04	568
40.00	26	100.00	7.792E-04	8.267E-04	827
60.14	40	59.73	5.836E-04	5.604E-04	560

Figure B-7: Results from ABAQUS simulations. Ranges from 450-800 nm

$$k_{axial} = \frac{12EI}{L^3}$$

$$k_{axial}$$

$$J\ddot{\theta} = \tau - 2k_{axial}r^2\theta$$

Static analysis $\quad 0 = \tau - 2k_{axial}r^2\theta$

$$\tau = \underbrace{2k_{axial}r^2}_{k_{rot}}\theta$$

$$k_{rot} = 2k_{axial}r^2$$
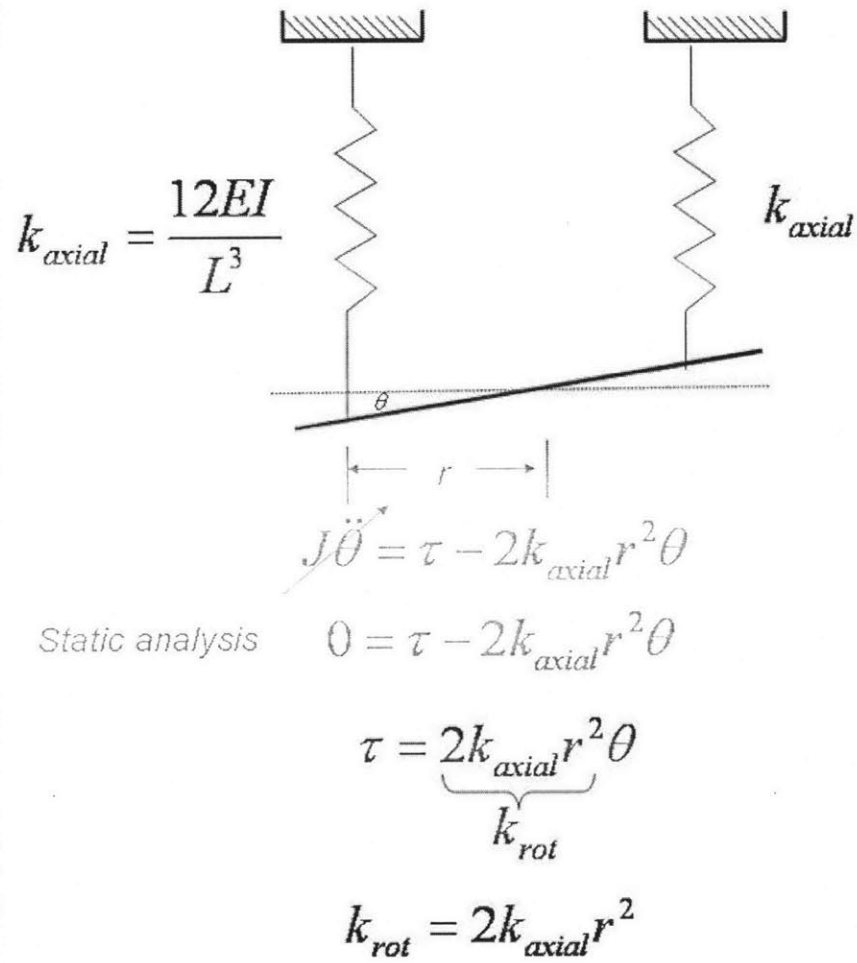
Figure B-8: Rotational stiffness of two double parallelograms in parallel

B.4 MATLAB Code

```
% Justin Lai

% Mechatronics Research Lab

% Code to consider the stiffnesses of the system


E = 70e9;                  %Pa

b = 1*25.4e-3;             %m, thickness of system

h = .75*25.4e-3            %m, width of post

A = b*h;                   %m^2, cross sectional area


L_post = 2*25.4e-3;

t_post = .2*25.4e-3;

r_post = 25.4e-3*[.1:.01:.2];

r_post_disp = r_post/25.4e-3;


k_axial = E*A/L_post;          %N/m^2, axial stiffness of post

k_notch = 2*E*b*t_post.^(5/2)./(9*pi*sqrt(r_post));


d_top = 6*25.4e-3;         %diameter of upper plate

L_arm = d_top/2;


alpha = 2e-3;              %milliradians


theta_error = (k_notch./k_axial)*(alpha/L_arm.^2);

figure(1)

plot(r_post_disp, theta_error)

title('Changing Radius of notch, theta-error')

xlabel('radius of post (in)')

ylabel('Error (milliradians)')
```

```
L_post = 25.4e-3*[1:.1:3];       %m

L_post_disp = L_post/25.4e-3;


k_axial = E*A./L_post;           %N/m^2, axial stiffness of post


t_post = .2*25.4e-3;          %
r_post = .15*25.4e-3;         %
k_notch = 2*E*b*t_post.^(5/2)./(9*pi*sqrt(r_post));


theta_error = (k_notch./k_axial).*(alpha./L_arm.^2);
figure(2)
plot(L_post_disp, theta_error)
title('Changing Length of post, theta-error')
xlabel('Length of post (in)')
ylabel('Error (milliradians)')
%%%%%%%%%%%
[L_post,r_post] = meshgrid([1:.1:3],[.1:.01:.2]);
[L_post2,r_post2] = meshgrid(25.4e-3*[1:.1:3],25.4e-3*[.1:.01:.2]);
L_post_disp1 = L_post(1,:);
r_post_disp1 = r_post(1,:);
L_post_disp2 = L_post2(1,:)/25.4e-3;
r_post_disp2 = r_post2(1,:)/25.4e-3;
k_axial = E*A./L_post2;          %N/m^2, axial stiffness of post


t_post = .2*25.4e-3;          %
k_notch = 2*E*b*t_post.^(5/2)./(9*pi*sqrt(r_post2));


theta_error = (k_notch./k_axial).*(alpha./L_arm.^2);
```

```
figure(3)
surf(L_post,r_post,theta_error)
xlabel('Length of post (in)')
ylabel('radius of notch (in)')
zlabel('theta-error')
title('Length arm 3 inches')
%%%%%%%%%%%%%%%%%%
```

THIS PAGE INTENTIONALLY LEFT BLANK

Bibliography

[1] S. Awtar. *Synthesis and Analysis of Parallel Kinematic XY Flexure Mechanisms.* PhD thesis, Massachusetts Institute of Technology, 2004.

[2] S. Awtar and A. H. Slocum. Fabrication, assembly, and testing of a new x-y flexure stage with substantially zero parasitic error motions. Technical report, Massachusetts Institute of Technology, 2004.

[3] S. Awtar and A. H. Slocum. In-plane capacitance probeholding mechanism. Technical report, Massachusetts Institute of Technology, 2004.

[4] S. Awtar and A. H. Slocum. Planer flexure mechanisms with two, three, or five degrees of freedom. Technical report, Massachusetts Institute of Technology, 2004.

[5] B. J. Choi, S. V. Sreenivasan, S. Johnson, M. Colburn, and C. G. Wilson. Design of orientation stages for step and flash imprint lithography. *Precision Engineering*, 25(3):192–199, 2001.

[6] M.L. Culpepper and G. Anderson. Design of a low-cost nano-manipulator which utilizes a monolithic, spatial compliant mechanism. *Precision Engineering*, 28(4):469–482, 2004.

[7] M. Gutierrez. Size adjustable separation for biologically active molecules. Master's thesis, Massachusetts Institute of Technology, 2004.

[8] M. Gutierrez and K. Youcef-Toumi. Programmable separation for biologically active molecules. In *ASME IMECE*, Chicago, IL, November 2006. ASME IMECE. IMECE2006-14141.

[9] L.L. Howell. *Compliant Mechanisms*. Wiley and Sons, 2001.

[10] H. J. Issaq. The role of separation science in proteomics research. *Electrophoresis*, 22(17):3629–3638, 2001.

[11] K. Joulain, J. Mulet, F. Marquier, R. Carminati, and J. Greffet. Surface electromagnetic waves thermally excited: Radiative heat transfer, coherence properties and casimir forces revisited in the near field. *Surface Science Reports*, 57(3-4):59–112, 2005.

[12] A.M. Kendale. Automation of soft lithographic microcontact printing. Master's thesis, Massachusetts Institute of Technology, 2002.

[13] J.B. Koelsch. Waterjet vs. edm. *Manufacturing Engineering*, 135(1), 2005.

[14] OMAX. Minimizing water jet taper. Available at http://www.omax.com/taper.php. 2007. 21409 72nd Ave South. Kent. WA 98032.

[15] V. Shilpiekandula. Progress through mechanics: Small-scale gaps. *Mechanics [Publication of American Academy of Mechanics]*, 35(9-10):3–6, September-October 2006.

[16] V. Shilpiekandula and K. Youcef-Toumi. Modeling and control of a programmable filter for separation of biologically active molecules. *American Control Conference, 2005. Proceedings of the 2005*, pages 394–399, 2005.

[17] V. Shilpiekandula and K. Youcef-Toumi. Design and control of programmable small-scale gaps: A progress report. Technical report, Massachusetts Institute of Technology, 2006.

[18] A. H. Slocum. *Precision Machine Design*. Society of Manufacturing Engineers, 1992.

[19] S.T. Smith. *Flexures: elements of elastic mechanisms.* Gordon and Breach, 2000.

[20] M. C. S. Tam, S. Payandeh, and A. M. Parameswaran. Design and development of a multiple dof compliant robot. *Advanced Robotics, 2005. ICAR '05. Proceedings., 12th International Conference on,* pages 876–881, 2005.

[21] S. Woody and S. Smith. Design and performance of a dual drive system for tip-tilt angular control of a 300 mm diameter mirror. *Mechatronics,* 16(7):389–397, 2006.

[22] A. A. Yu, T. A. Savas, G. S. Taylor, A. Guiseppe-Elie, H. I. Smith, and F. Stellacci. Supramolecular nanostamping: Using dna as movable type. *Nano Letters,* 5(6):1061–1064, 2005.